LETTER

Infrared light emission from nano hot electron gas created in atomic point contacts

A Letters Journal Exploring the Frontiers of Physics

June 2016

EPL, **114** (2016) 57002
doi: 10.1209/0295-5075/114/57002

www.epljournal.org

Infrared light emission from nano hot electron gas created in atomic point contacts

T. Malinowski, H. R. Klein, M. Iazykov and Ph. Dumas

Aix Marseille Université, CNRS, CINaM UMR 7325 - 13288, Marseille, France

received 10 March 2016; accepted in final form 13 June 2016
published online 4 July 2016

PACS 73.63.Rt – Electronic transport in nanoscale materials and structures: Nanoscale contacts
PACS 78.67.Bf – Optical properties of low-dimensional, mesoscopic, and nanoscale materials and structures: Nanocrystals, nanoparticles, and nanoclusters

Abstract – Gold atomic point contacts are prototype systems to evidence ballistic electron transport. The typical dimension of the nanojunction being smaller than the electron-phonon interaction length, even at room temperature, electrons transfer their excess energy to the lattice only far from the contact. At the contact however, favored by huge current densities, electron-electron interactions result in a nano hot electron gas acting as a source of photons. Using a home built Mechanically Controlled Break Junction, it is reported here, for the first time, that this nano hot electron gas also radiates in the infrared range (0.2 eV to 1.2 eV). Moreover, following the description introduced by Tomchuk *et al.* (*Sov. Phys.-Solid State*, **8** (1966) 2510), we show that this radiation is compatible with a black-body–like spectrum emitted from an electron gas at temperatures of several thousands of kelvins.

Introduction. – Understanding and managing the interplay between electrons and photons around the Fermi level is of paramount importance for both fundamental and applied solid-states physics [1]. The recent intense research works in the field of nanoantennas [2] or regarding light-emitting diode droop (see [3], and references therein) illustrate this importance. As the sizes of the active regions shrink to the nanometre scale, as local current densities increase, new processes, previously not favoured, are put forward, intentionally or not.

The tip of a scanning tunneling microscope has been used to inject electrons and to promote local light emission from semiconductor quantum structures [4–6] or from single molecules [7]. These STM light emission (STM-LE) works followed the pioneering work of Gimzewski's group on metals [8,9]. For metals, in the 10^{-4} G_0 conductance range ($G_0 = 2e^2/h$), the well-accepted dominant one-electron mechanism is the following [10]: an inelastic tunneling electron excite collective electron modes of the gap mode plasmon resonator. These modes depend on the geometry of the cavity at the nanoscale and on the dielectric properties of the metals [11]. These electromagnetic modes relax their energy mainly to the phonons but also through photon emission. The two key features of the emitted spectra are i) that they exhibit plasmonic resonances typical of the cavity and metals-dependent, and ii) that the high-energy part of the spectra is limited by the energy carried by a tunneling electron ($h\nu \leqslant$ eV) [12]. Although it is obviously not possible to know the tip shape at this scale, and thus the electromagnetic modes due to the gap mode plasmons, it has been shown that rationalizing spectra acquired with the same tip on different areas or at different bias conditions could provide useful physical information, respectively, on the material below the tip [7,13] or on the carrier density [14].

Indeed photons with energies exceeding the so-called quantum cutoff "limit" of $h\nu = eV$ have also been observed in the STM-LE regime [15,16]. Such photon energies are still observed at higher conductances, above G_0 in the Atomic Point Contact Light Emission (APC-LE) regime [17,18]. The emission of these photons evidences the multi-carrier excitation process.

During the last decades, atomic-sized metallic conductors have been extensively studied [19], a prototype system being the well-known stretched gold nanowire. Under bias, prior to being broken, the conductance of such a wire exhibits characteristic Landauer plateaus at integer multiples of G_0 [20,21]. Along these plateaus the conductance remains constant despite the length increase of the metallic nanowire. Indeed, as long as the length of the nanoconstriction is much smaller than the electron-phonon interaction length $L_{e\text{-}ph}$ [22], no extra-resistance

is added to the contact resistance. Moreover, considering only electron-phonon scattering, the electron injected from one contact to the other will preserve its energy and momentum over ballistic distances of the order of $L_{e\text{-}ph}$. An order of magnitude of $L_{e\text{-}ph}$ can be estimated from:

$$L_{e\text{-}ph} = \frac{v_F}{\omega_D \gamma} \tag{1}$$

with v_F the Fermi velocity, ω_D the Debye frequency and γ, the electron-phonon coupling factor ($\gamma < 1$) [22].

However, these gold nanoconstrictions are the siege of huge current densities ($|\vec{j}| \simeq 10^{15}\,\mathrm{A \cdot m^{-2}}$) and electron-electron interactions play a significant role in redistributing the energy of the electrons [23].

As mentioned above, light emission from APC is also observed. The spectra show the presence of photons with energy $h\nu$ above the polarisation energy eV of electrons [17,18,24]. The emission of these photons evidences the role of multi-carrier excitation processes resulting in a hot-carrier energy distribution spreading above eV.

From their first observations, Downes *et al.* [17] have put forward the radiative emission from of a hot electron gas. Consistently with previous works on systems with similar physics (see [25] and references therein), electron temperatures of the order of 2000 K were extrapolated fitting the corrected emission spectra by a black-body behaviour. Applying a 1 volt bias, at a conductance of 1 G_0, photons with energy above 2.5 eV were detected. Although most spectra were featureless in the visible range, modulation or intense peaks, evoking electromagnetic resonances of the gap mode plasmons were sometimes observed. These experiments were performed with an STM in ultra-high vacuum (UHV), at 300 K.

In similar conditions, but at 4 K, Schull *et al.* [18] also reported light emission above the quantum cutoff. However, their results are different from two important points of view: i) spectra exhibit resonance features similar to what is commonly observed in STM-LE and ii) no photon of energy above twice eV is observed. The high-energy part of the spectra is also attributed to hot electrons, hotter than eV, excited through an Auger-like two charge carriers cascade mechanism. We note that this mechanism is fully consistent with photon energies between eV and 2 eV, as observed in [18], but this mechanism could also be recursive and easily account for photon emission above 2 eV.

Recently, Buret *et al.* [24] also reported black-body–like emission from electroformed gold junction at conductance values of the order of G_0. As in [17], they also observed photons with energy above 2 eV consistently with a black-body–like radiation of a hot electron gas. Electronic temperatures, T_e, above 1500 K, *i.e.* well above the gold melting point ($T_m = 1338$ K), are indirectly measured. To explain the apparent experimental discrepancy with [18], they propose a mechanism involving gold interband reabsorption by low-lying *d*-band electrons.

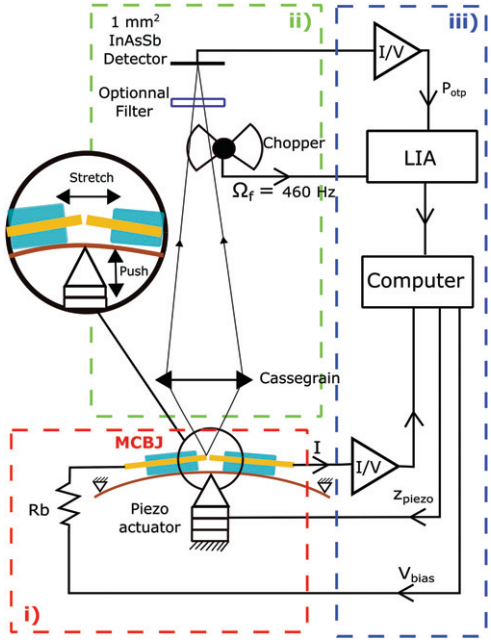

Fig. 1: (Colour online) Experimental set-up. i) MCBJ with a piezo actuator. Photons are collected using a reflective Cassegrain objective ($15\times$, NA = 0.5), optionally filtered and chopped at 460 Hz and detected using a cooled InAsSb IR detector. ii) The magnified view shows the MCBJ principle (push-to-stretch movement). The control and acquisition electronic consists of a current-voltage convertors, a lock-in amplifier (LIA) and a computer.

Using a home-build Mechanical Controlled Break Junction (MCBJ) [26], we have been revisiting APC-LE both in the visible range and, for the first time, in the near-infrared (IR) range of the spectrum. This article focuses on the IR range. We report intense IR emission, conterbalancing the known relatively poor sensitivity of IR detectors. We also report basic spectroscopic data, supporting a black-body–like emission from hot electron gas.

One of the reasons for focusing on the emission in the IR range is that we do not expect electromagnetic plasmonic resonances comparable to what is observed in the visible range. In the classical theory [11] we would expect a diverging redshift of these resonances as the distance between electrodes is reduced from the STM regime down to the contact regime. Noteworthy, to our knowledge, this redshift was never observed. Indeed, recent quantum approaches, including tunneling between the electrodes, have theoretically predicted [27,28] and experimentally demonstrated [28] a non-monotonous behaviour, limiting the wavelength of the resonances below 1 micron.

Experimental set-up. – For these experiments, the setup consists of i) a MCBJ, ii) the light collection and detection components and iii) the acquisition and control electronics and informatics (see fig. 1). The MCBJ was first introduced by Van Ruitenbeek *et al.* [29]. For these studies, our one is operated in air and at room temperature. The mechanical part is similar to the one we

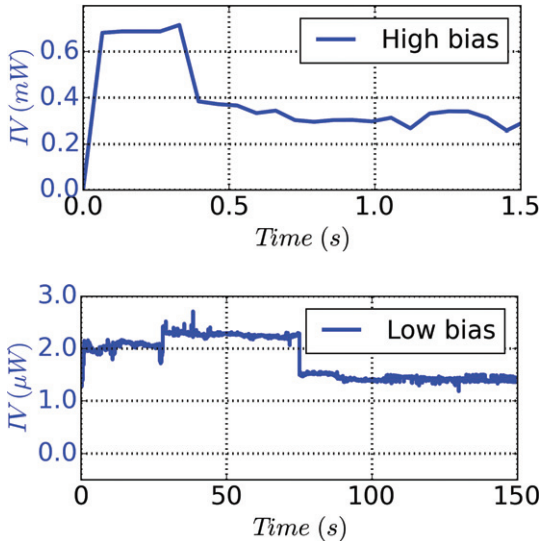

Fig. 2: (Colour online) Temporal evolution of IV, the electrical power, without feedback. Top: high-bias regime ($V_{bias} = 1.5\,\mathrm{V}$, $G \simeq 3\ G_0$ for $IV \simeq 300\,\mu\mathrm{W}$). Bottom: low-bias regime ($V_{bias} = 0.139\,\mathrm{V}$, $G \simeq 1\ G_0$ for $IV \simeq 1.5\,\mu\mathrm{W}$).

described previously [26], although the sample preparation technique has been since improved. The separation of the electrodes is controlled by a micrometer step motor stacked-up with a piezoelectric actuator (sensitivity: $216\,\mathrm{nm}\cdot\mathrm{V}^{-1}$). Motor and piezo are driven through an input/output (IO) board by a computer interface, that is also used for acquiring data and feedbacking (see below). Taking into account a typical push:stretch ratio of 20:1 and the resolution of our 16-bit DAC, one digit corresponds to less than 3 pm which is quite enough for this work. Assuming an ohmic behaviour of the gold nanojunction as reported in the litterature [30,31], the conductance is derived from the measured intensity that flows through the junction using a current/voltage converter (DLPCA-200, FEMTO) with a $10^4\,\mathrm{A/V}$ transconductance gain. At low bias ($V_{bias} \simeq 130\,\mathrm{mV}$), in air and at room temperature, atomic contacts often remain stable for tens of seconds [26]. Figure 2 illustrates the long-term stability of junctions biased at low voltage. As the bias is increased up to values stimulating light emission, the lifetime of monoatomic contacts decreases drastically, as we will see below.

To collect infrared photons, we are using a Cassegrain microscope objective ($\times 15$; NA = 0.5). The optical beam is mechanically chopped at 460 Hz, transmitted through a semiconductor filter and measured by a cooled InAsSb detector (P11120-201, Hamamatsu) sensitive from 0.2 eV to 1.2 eV, using a lock-in amplifier (HF2LI, Zurich Instruments). We use silicon and germanium wafers of respective gap 1.12 eV and 0.68 eV as low-pass filters to gather rudimentary spectroscopic data.

To measure an optical IR signal we operate with an input electrical power in the mW range. More precisely, we apply a bias in the volt range and drive the MCBJ

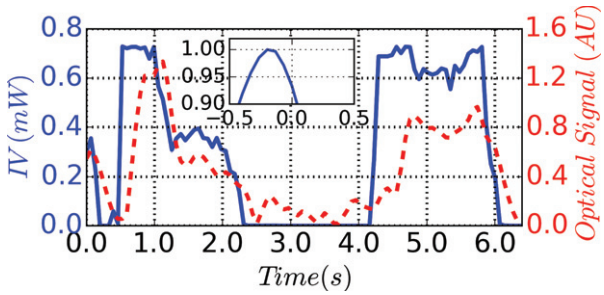

Fig. 3: (Colour online) Temporal evolutions of the electrical power IV (blue line) and optical signal (red dashed line). The delay is due to the chosen LIA time constant. It can be quantified by the cross-correlation (see inset).

at a conductance of a few G_0. The MCBJ device is mechanically and thermally stable at the macroscopic scale. Moreover, taking advantage of thermal diffusion and electromigration, at room temperature, the nanojunction self-organises at atomic level and naturally explores the more stable configurations around the average chosen conductance value. We thus only need a loose feedback using the piezo actuator to maintain the conductance between 0.5 and 20 G_0.

Results. – Since we deliberately drive our MCBJ in a loose feedback mode, its conductance naturally varies during the experiments. We have plotted (fig. 2) the temporal evolution of electrical power IV, which is a relevant parameter [25]. It shows that the applied bias and the stability are negatively correlated. A compromised to measure an optical signal thus has to be found.

Figure 3 plots together the temporal evolution of the measured electrical power and optical signal. The response, measured without low-pass optical filters, appears to be strongly correlated with the electrical power injected in the junction and slightly time-delayed. Cross-correlation (fig. 3, inset) of both signals allows to quantify this time lag due to the integration time of the optical signal.

The important result at this point is that an IR signal emitted from the APC is detected. Noteworthy, a signal is detected despite the low sensitivity of optical sensors in the IR range, compared with the sensitivity of sensors in the visible range.

Taking into account the time lag, fig. 4 shows the dependence of the optical signal with the electrical power injected in the APC. The red continuous line is the modelled dependence of the IR signal assuming black-body emission as previously proposed [17]. We will come back to this point in the "Discussion" section.

These data are acquired using the full spectral bandwidth of the IR detector. To get some basic spectroscopic information we use semiconductor low-pass filters. The smaller the gap the narrower the optical bandwidth. Table 1 shows the results acquired in the mW regime ($V = 0.9\,\mathrm{V}$, $I = 720\,\mu\mathrm{A}$).

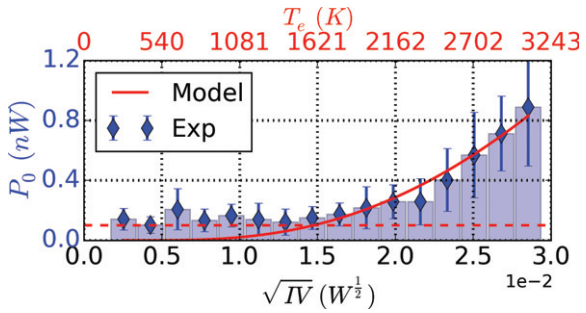

Fig. 4: (Colour online) Experimental (blue columns) and calculated (red continus line) dependences of the optical power P_0 with $\sqrt{IV}$. Blue columns correspond to the mean value of the optical power over a binned x-axis. Error bars show the standard deviation calculated over the same binned x-axis. The calculated continous line allows the determination of the equivalent hot electrons temperature T_e shown on the top x-axis (see discussion section). The dashed horizontal red line represents the noise floor of the optical detector. Data for this figure come from 150 nanojunctions, each of them lasting a few seconds.

Table 1: Optical signal measured using different semiconductors as low-pass filters.

Filters	Raw data (AU)
Full output	1.05 ± 0.04
Si gap = 1.12 eV	0.95 ± 0.08
Ge gap = 0.68 eV	0.56 ± 0.06

Table 2: Relative integrated optical signals measured and calculated over the three spectral bands. Detector sensitivity is taken into account.

Spectral Bands (eV)	Measurement	Calculus
Full band = 0.22 1.2	1	1
0.22 0.68	0.56 ± 0.06	0.61
0.68 1.12	0.37 ± 0.14	0.33
1.12 1.2	0.08 ± 0.12	0.058

The data reported in table 1 evidences that half of the signal arises from photons with energies lower than the Ge band gap. From this table, by difference, we construct table 2 to get the proportion of signal in each three spectral bands. Table 2 also includes a column of computed values that will be described in the discussion.

Figure 5 shows a black-body spectrum ($T = 2931$ K), convoluted by the detector spectral response. The three different spectral bands corresponding to the use of the optical filters are represented by grey-scale bands below the black-body spectrum. Integrating the optical signal for these 3 spectral bands allows the calculation of the expected 3 values reported in the appropriate column of table 2.

Discussion. – As mentioned above, APC-LE has been attributed to the radiation from a hot electron gas [17,18,24]. The associated observed spectrum was

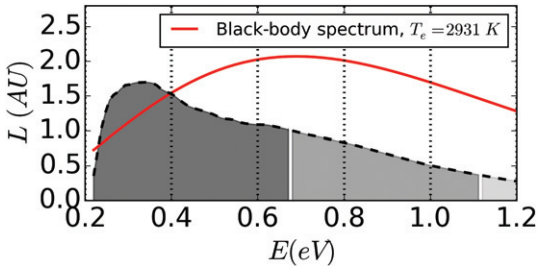

Fig. 5: (Colour online) Calculated emission (red line) and detected (black dashed line) spectra, taking into account the detector spectral response. The black-body temperature is assumed to be 2931 K. Grey scale bands show the spectral bands defined by the semiconductors filters used to gather the integrated optical signal.

proposed to correspond to a black-body–like emission from a high-temperature (T_e) system [17,24,25]. Such an emission spectrum obeys

$$L(E, T_e) = \frac{2}{(hc)^2} \frac{E^3}{\exp\left(\frac{E}{k_B T_e}\right) - 1} \tag{2}$$

with $L(E, T_e)$ being the optical luminance, T_e the temperature, E the photon energy, k_b the Boltzmann constant, h the Planck constant and c the light velocity. Tomchuk and Fedorovich showed [1] that the electronic temperature in isolated metal island, with dimension below $L_{e\text{-}ph}$, could be related to the lattice temperature T_L and electrical power following the equation:

$$(k_B T_e)^2 = (k_B T_L)^2 + \alpha IV. \tag{3}$$

Here I is the current and V the applied bias and α is an empirical constant describing the heating efficiency. Assuming $T_L \ll T_e$, we can write

$$L(E, IV, \alpha) = \frac{2}{(hc)^2} \frac{E^3}{\exp\left(\frac{E}{\sqrt{\alpha IV}}\right) - 1}. \tag{4}$$

Taking into account the spectral response $F(E)$ and bandwidth of the detector, integrating the optical luminance and normalizing, we compute the optical power $P_0(IV, \alpha)$:

$$P_0(IV, \alpha) = \int_{E_{min}=0.22\,\mathrm{eV}}^{E_{max}=1.2\,\mathrm{eV}} F(E) L(E, IV, \alpha)\, \mathrm{d}E \tag{5}$$

The continuous red line of fig. 4 is computed from this expression, α being the only fitting parameter. The fit was obtained for $\alpha = 0.014\hbar$.

From the fitted α and measured IV values we can calculate the electronic temperature from $k_B T_e = \sqrt{\alpha IV}$. This T_e values are reported on the top axis of fig. 4. In standard operating conditions of the MCBJ (*i.e.* conductance of a few G_0), T_e of several thousands of degrees, far exceeding T_L, are found and fortify the above assumptions.

From an experiment corresponding to $IV = 1.1$ mW, knowing the fitted α value an thus the hot electron gas

temperature using eq. (3) we plot the expected black-body spectrum (fig. 5 red continuous curve).

From it, taking into account the detector response and the above-mentionned bandwidths (BW) of the three low-pass optical filters, we compute the three normalised optical powers, using

$$P(IV, \alpha, BW) = \frac{\int_{BW} F(E) L(E, IV, \alpha)\, \mathrm{d}E}{P_0(IV, \alpha)} \qquad (6)$$

with BW being the bandwidth of the considerate spectral band. These computed values are reported in the last column of table 2.

This leads to an excellent agreement between the measured and calculated values for all three bands. We point out that, although basic, the spectroscopic analysis gives very useful results corroborating the black-body model of the emission source.

Moreover the proportion of signal below and above the germanium bandgap can only be consistent with black-body temperatures far above the Au melting temperature.

Conclusion and perspectives. – In this letter, we have reported for the first time the observation of IR light emission from metallic point contacts. Results are quantitatively consistent with the emission of a hot electron gas the temperature of which exceeds the melting point of gold.

Results also prolongate the conclusions previously made, at lower input power on the basis of the light detected in the visible range, by Downes *et al.* [17] and by Buret *et al.* [24]. The spectroscopic analysis is already very useful and we forecast that in a near future the stability of APC at ambient temperature will allow to use more advanced and enlightening tools (such as Fourier Transform InfraRed spectroscopy).

* * *

We would like to thank Mehdi Lagaize for helpful technical support.

REFERENCES

[1] Tomchuk P. M. and Fedorovich R. D., *Sov. Phys.-Solid State*, **8** (1966) 2510.

[2] Novotny Lukas and Van Hulst Niek, *Nat. Photon.*, **5** (2011) 83.

[3] Iveland Justin, Martinelli Lucio, Peretti Jacques, Speck James S. and Weisbuch Claude, *Phys. Rev. Lett.*, **110** (2013) 177406.

[4] Renaud Philippe and Alvarado Santos F., *Phys. Rev. B*, **44** (1991) 6340.

[5] Ushioda S., Tsuruoka T. and Ohizumi Y., *Appl. Surf. Sci.*, **166** (2000) 284.

[6] Dumas Ph., Derycke V., Makarenko I. V., Houdre R., Guaino P., Downes A. and Salvan F., *Appl. Phys. Lett.*, **77** (2000) 3992.

[7] Qiu X. H., Nazin G. V. and Ho W., *Science*, **299** (2003) 542.

[8] Gimzewski J. K., Reihl B., Coombs J. H. and Schlittler R. R., *Z. Phys. B: Condens. Matter*, **72** (1988) 497.

[9] Gimzewski J. K., Sass J. K., Schlitter R. R. and Schott J., *Europhys. Lett.*, **8** (1989) 435.

[10] Berndt Richard, Gimzewski James K. and Johansson Peter, *Phys. Rev. Lett.*, **67** (1991) 3796.

[11] Rendell R. W. and Scalapino D. J., *Phys. Rev. B*, **24** (1981) 3276.

[12] Coombs J. H., Gimzewski J. K., Reihl B., Sass J. K. and Schlittler R. R., *J. Microsc.*, **152** (1988) 325.

[13] Downes Andrew, Guaino Philippe and Philippe Dumas, *Appl. Phys. Lett.*, **80** (2002) 380.

[14] Schneider N. L., Matino F., Schull G., Gabutti S., Mayor M. and Berndt R., *Phys. Rev. B*, **84** (2011) 153403.

[15] Pechou R., Coratger R., Ajustron F. and Beauvillain J., *Appl. Phys. Lett.*, **72** (1998) 671.

[16] Hoffmann Germar, Berndt Richard and Johansson Peter, *Phys. Rev. Lett.*, **90** (2003) 046803.

[17] Downes A., Dumas Ph. and Welland M. E., *Appl. Phys. Lett.*, **81** (2002) 1252.

[18] Schull Guillaume, Nel Nicolas, Johansson Peter and Berndt Richard, *Phys. Rev. Lett.*, **102** (2009) 057401.

[19] Agrait Nicolas, Levy Yeyati Alfredo and van Ruitenbeek Jan M., *Phys. Rep.*, **377** (2003) 81.

[20] Yanson A. I., Rubio Bollinger G., Van den Brom H. E., Agrait N. and Van Ruitenbeek J. M., *Nature*, **395** (1998) 783.

[21] Leoni Thomas, Zoubkoff Remi, Homri Sabrina, Candoni Nadine, Vidakovic Petar, Ranguis Alain, Klein Hubert, Saul Andres and Dumas Philippe, *Nanotechnology*, **19** (2008) 355401.

[22] Ashcroft Neil W. and David Mermin N., *Solid State Physics* (Saunders, Philadelphia) 1976, p. 293.

[23] Pierre F., Pothier H., Esteve D. and Devoret M. H., *J. Low Temp. Phys.*, **118** (2000) 437.

[24] Buret Mickael, Uskov Alexander V., Dellinger Jean, Cazier Nicolas, Mennemanteuil Marie-Maxime, Berthelot Johann, Smetanin Igor V., Protsenko Igor E., Colas des Francs Grard and Bouhelier Alexandre, *Nano Lett.*, **15** (2015) 5811.

[25] Fedorovich R. D., Naumovets A. G. and Tomchuk P. M., *Phys. Rep.*, **328** (2000) 73.

[26] Alwan Monzer, Candoni Nadine, Dumas Philippe and Klein Hubert R., *Eur. Phys. J. B*, **86** (2013) 243.

[27] Romero Isabel, Aizpurua Javier, Bryant Garnett W. and García De Abajo F. Javier, *Opt. Express*, **14** (2006) 9988.

[28] Savage Kevin J., Hawkeye Matthew M., Esteban Rubén, Borisov Andrei G., Aizpurua Javier and Baumberg Jeremy J., *Nature*, **491** (2012) 574.

[29] Van Ruitenbeek J. M., Alvarez A., Pineyro I., Grahmann C., Joyez P., Devoret M. H., Esteve D. and Urbina C., *Rev. Sci. Instrum.*, **67** (1996) 108.

[30] Boussaad S. and Tao N. J., *Appl. Phys. Lett.*, **80** (2002) 2398.

[31] Nielsen S. K., Brandbyge M., Hansen K., Stokbro K., van Ruitenbeek J. M. and Besenbacher F., *Phys. Rev. Lett.*, **89** (2002) 066804.